Conformal Coverage of Poly(3,4-ethylenedioxythiophene) Films with Tunable Nanoporosity *via* Oxidative Chemical Vapor Deposition

Sung Gap Im,[†] David Kusters,[‡] Wonjae Choi,[§] Salmaan H. Baxamusa,[†] M. C. M. van de Sanden,[‡] and Karen K. Gleason[†,*]

[†]Department of Chemical Engineering and Institute for Soldier Nanotechnologies, Massachusetts Institute of Technology, Cambridge, Massachusetts 02139, [‡]Department of Applied Physics, Eindhoven University of Technology, Eindhoven, The Netherlands, and [§]Department of Mechanical Engineering, Massachusetts Institute of Technology, Cambridge, Massachusetts 02139

ABSTRACT Novel nanoporous poly(3,4-ethylenedioxythiophene) (PEDOT) films with basalt-like surface morphology are successfully obtained *via* a one-step, vapor phase process of oxidative chemical vapor deposition (oCVD) by introducing a new oxidant, $CuCl_2$. The substrate temperature of the oCVD process is a crucial process parameter for controlling electrical conductivity and conjugation length. Moreover, the surface morphology is also systemically tunable through variations in substrate temperature, a unique advantage of the oCVD process. By increasing the substrate temperature, the surface morphology becomes more porous, with the textured structure on the nanometer scale. The size of nanopores and fibrils appears uniformly over 25 mm × 25 mm areas on the Si wafer substrates. Conformal coverage of PEDOT films grown with the $CuCl_2$ oxidant (C-PEDOT) is observed on both standard trench structures with high aspect ratio and fragile surfaces with complex topology, such as paper, results which are extremely difficult to achieve with liquid phase based processes. The tunable nanoporosity and its conformal coverage on various complex geometries are highly desirable for many device applications requiring controlled, high interfacial area, such as supercapacitors, Li ion battery electrodes, and sensors. For example, a highly hydrophilic surface with the static water contact angle down to less than 10° is obtained solely by changing surface morphology. By applying fluorinated polymer film onto the nanoporous C-PEDOT *via* initiative chemical vapor deposition (iCVD), the C-PEDOT surface also shows the contact angle higher than 150°. The hierarchical porous structure of fluorinated polymer coated C-PEDOT on a paper mat shows superhydrophobicity and oil repellency.

KEYWORDS: poly(3,4-ethylenedioxythiophene) (PEDOT) · oxidative chemical vapor deposition (oCVD) · oxidant · $CuCl_2$ · $FeCl_3$ · nanostructure · conformal coverage · superhydrophobicity · oleophobicity

Nanostructured materials have drawn significant research interest as their properties are often unique with respect to bulk materials of identical chemical composition.[1] Controlling the properties of these materials requires structural control on the nanometer scale.[2] A number of chemical and physical methodologies have been applied to synthesize nanostructured metals, inorganics, polymers, and carbon nanotubes, having a variety of potential applications, including circuit integration, microfluidics, and biomedical devices.[3,4]

Conducting polymers are regarded as one of the most promising materials for nanostructured devices.[5,6] Poly(3,4-ethylenedioxythiophene) (PEDOT) is a particularly interesting conducting polymer due to its excellent environmental stability and high optical transparency in its electrically conductive state.[7,8] Moreover, since it has a moderate band gap with low redox potential and exceptionally high conductivity, PEDOT has been applied to various electronic devices such as electrochemical cells,[7] chemical sensors,[9,10] and transparent, flexible electrodes for organic electronics.[11] Currently, nanostructured PEDOT has been reported using various synthesis schemes.[5] For example, Jang *et al.* fabricated PEDOT nanorods for a sensing application by using micelle intermediated interfacial oxidative polymerization.[9] Abidian *et al.* synthesized PEDOT nanotubes for controlled drug release by utilizing electrospun fibers as a template in electrochemical polymerization.[12] However, these synthetic methodologies require multistep procedures and strict control over reaction conditions.

Previously, we have demonstrated an *in situ* deposition of well-defined, optically transparent PEDOT films on a variety of substrates, including Si wafers, paper, aluminum foil, and plastic substrates by using oxidative chemical vapor deposition (oCVD).[13−16] The oCVD film growth was achieved through vapor phase introduction of both the oxidant, $FeCl_3$, and the monomer, 3,4-ethylenedioxythiophene

*Address correspondence to kkg@mit.edu.

Received for review June 16, 2008 and accepted August 19, 2008.

Published online August 28, 2008. 10.1021/nn800380e CCC: $40.75

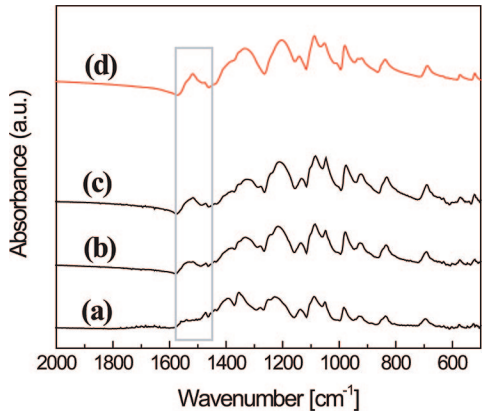

Figure 1. FTIR spectra of PEDOT films *via* oCVD process with (a−c) $CuCl_2$ or (d) $FeCl_3$ as an oxidant; (a) T_{sub} = 20 °C, conductivity was 0.22 S/cm; (b) T_{sub} = 50 °C, conductivity was 3.3 S/cm; (c) T_{sub} = 80 °C, conductivity was 11.3 S/cm; (d) T_{sub} = 55 °C, conductivity was 11.2 S/cm. The rectangle highlights an absorption region associated with conjugation in the oCVD PEDOT.

(EDOT). The electrical conductivity, doping level, and work function of the oCVD PEDOT could be controlled by varying substrate temperature (T_{sub}),[13,14] and the maximum electrical conductivity achieved was greater than 700 S/cm.[13,15] The oCVD PEDOT could also be grafted on various organic plastic substrates such as polystyrene (PS), polycarbonate (PC), and polyethyleneterephthalate (PET).[15]

In this report, we describe a new synthetic scheme to fabricate nanoporous, basalt-like PEDOT films by introducing a new oxidant, $CuCl_2$, to the oCVD process. Both $CuCl_2$ and $FeCl_3$ are oxidants which are categorized as Friedel−Crafts catalysts.[15] The surface morphology and nanostructure of the resultant films could be systematically controlled by changing T_{sub}. The nanostructured PEDOT could also be conformally coated on various geometries, including trenches with high aspect ratio and complex, fragile surfaces without damaging the subtle surface structure, which is difficult to achieve *via* a non-CVD process.[17] Water and ethanol droplet contact angles on these nanoporous PEDOT films showed that the contact angle was highly dependent on surface morphology. Superhydrophobicity and oleophobicity were also readily obtained *via* vapor phase, initiative chemical vapor deposition (iCVD) of fluorinated polymer film on nanostructured oCVD PEDOT. The size-tunable nanoporous PEDOT film has a high surface area and thus may find direct application in various devices that require high interfacial areas such as sensors, lithium secondary batteries, and supercapacitors.[8]

RESULTS AND DISCUSSION

FTIR Spectra. The Fourier transform infrared (FTIR) spectra of oCVD PEDOT with $CuCl_2$ as an oxidizing agent (C-PEDOT, afterward) at three different values of T_{sub} (Figure 1a−c) match the spectra for oCVD PEDOT with $FeCl_3$ as an oxidizing agent (F-PEDOT, afterward) at T_{sub} = 55 °C (Figure 1d). The detailed peak assignments were recently reported elsewhere.[13] This result indicates that $CuCl_2$ successfully oxidized the EDOT monomer to form PEDOT. Due to its insolubility, the molecular weight of PEDOT could not be measured with conventional methods such as gel-permeation chromatography (GPC).[13] However, compared to oligomeric PEDOT,[18] the peaks in the FTIR spectra of C-PEDOT are broadened by the doping effect,[19] which demonstrates that doped C-PEDOT was successfully polymerized. The intensity of the C═C[13,18] peak at 1520 cm^{-1} is known to increase as the conjugation length of PEDOT grows.[20] Thus, the gradual decrease in the intensity of the 1520 cm^{-1} peak as the substrate temperature decreases (Figure 1b and a) represents a decrease in the conjugation length of C-PEDOT. It is well-known that variation in conjugation length directly affects the electrical conductivity of PEDOT.[21] The increase in conjugation length and conductivity with increasing substrate temperature has also been observed in F-PEDOT[13,14] produced by oCVD. However, the absolute value of conductivity was highly affected by the oxidant used. For C-PEDOT, the maximum conductivity obtained was 32 S/cm at T_{sub} = 80 °C, which is almost one order lower than that of F-PEDOT.[13,15] Two possible reasons for this difference are lower oxidation potential of Cu^{2+} (E_0 = +0.153 eV) compared with Fe^{3+} (E_0 = +0.771 eV)[22] and the lower density of the oCVD films formed using $CuCl_2$, as will be discussed below.

Surface Morphology. The surface morphology of the C-PEDOT (Figure 2a−c) as imaged *via* scanning electron microscopy (SEM) differed from that of the smooth F-PEDOT (Figure 2d). F-PEDOT had a root mean squared (rms) roughness of less than 4 nm determined by atomic force microscopy (AFM). At the surface of F-PEDOT, shallow (<10 nm height) wrinkles of relative uniform spacing were also observed and are most likely formed by the reaction residue filtrated out from F-PEDOT during the rinsing process. On the other hand, the surface morphology of C-PEDOT is highly dependent on the substrate temperature used for film growth.

At T_{sub} = 20 °C, two distinct regions can be observed in C-PEDOT: a relatively dense and smooth area surrounding large, porous domains with rounded edges whose size ranges from *ca.* 200 to 300 nm diameters. Some of these porous domains merged to form larger regions having diameters of 500−1100 nm (Figure 2a, inset). At the higher T_{sub} of 50 °C, the surface morphology of C-PEDOT is highly interconnected and porous. The pore size ranged from 50 to 150 nm, and the diameter of the fibrils ranged between 40 and 100 nm. The relatively narrow size distribution of the nanopores and fibril structures was observed over the entire area of the 25 mm × 25 mm substrate. At T_{sub} = 80 °C, the surface morphology was similar to that at T_{sub} = 50 °C, but the film is more porous.

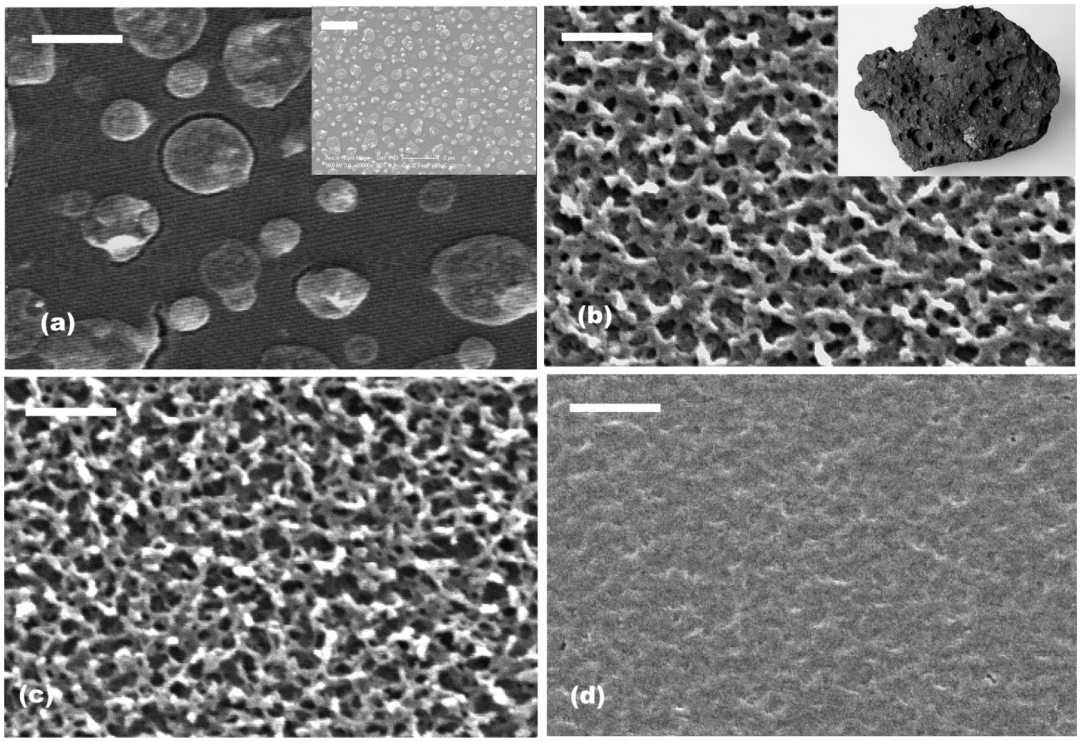

Figure 2. SEM images of (a−c) C-PEDOT and (d) F-PEDOT; (a) T_{sub} = 20 °C; (b) T_{sub} = 50 °C; (c) T_{sub} = 80 °C; (d) T_{sub} = 55 °C. Each scale bars represents 500 nm. Scale bar in the inset of (a) represents 5 μm. Inset of (b) is the digital camera image of basalt. Copyright (2008) by Andrew Alden, geology.about.com, reproduced under educational fair use.

The formation of pores in C-PEDOT is hypothesized to be related to the unique behavior of the $CuCl_2$ oxidant. The $CuCl_2$ is typically heated to temperatures of 380−420 °C inside a crucible located within the oCVD reactor. $CuCl_2$ is known to decompose to CuCl vapor and Cl_2 gas at temperatures higher than 300 °C.[23] While CuCl is known as a Lewis acid, its oxidation power is weak.[23] On the other hand, Cl_2 is a strong oxidant[23] and is capable of oxidizing the EDOT monomer to form a radical cation, the first step in the growth of conductive PEDOT chains. The vaporized CuCl is easily condensed at the substrate because it is essentially involatile at temperatures lower than 100 °C. On the other hand, Cl_2 is highly volatile (T_{bp} = −34.04 °C[22]) even at the lower temperature of the substrate. Since EDOT dimers and higher molecular weight EDOT oligomers are nearly involatile,[13] further step growth polymerization reactions are confined to the substrate. Therefore, a mixture of EDOT monomer, EDOT oligomers, and CuCl is formed on the relatively cold substrate. The CuCl at the substrate can be readily reoxidized to form $CuCl_2$ in the presence of oxidants, such as Cl_2 or residual O_2 in the reactor. Thus, the oxidative polymerization of EDOT can be performed by both Cl_2 and $CuCl_2$ at the surface of substrate. However, since Cl_2 is so volatile, it is likely that most of oxidation reactions at the surface of substrate are performed solely by $CuCl_2$. As $CuCl_2$ is a mild oxidant and the oxidation reaction is relatively slower than that of $FeCl_3$, the oxidative polymerization with $CuCl_2$ releases the gaseous reaction byproduct of HCl[13,16,24] more slowly than that with $FeCl_3$. Thus, the formation of bubbles in PEDOT film is most likely derived from the competing processes between the release of gaseous byproduct and the condensation of polymerized PEDOT film. If film has grown over the site of the release of the gaseous byproducts, the bubbles which eventually escape lead to the formation of pores. At low T_{sub}, the reaction is slow, allowing the entrapment of HCl vapor before the release of vapor occurs. Indeed in Figure 2a, corresponding to the lowest T_{sub} C-PEDOT, features resulting from gas evolution are observed only over part of the surface in island-like domains. The roughened surface inside these domains strongly implies the evolution of gas in this domain during the deposition process. The effused gas slowly forces the formation of expanded domains, and these bubbles collapse when the gas escapes. Each of the island domains contained at least one "vent-hole" through which the volatile gaseous component effused out. The observation from the magnified images supports the hypothesis that pores are formed by the outgassing of bubbles formed during the polymerization reaction.

The enlarged image of the inset of Figure 2a demonstrates that the morphology of the nodular structure is uniformly distributed. The size distribution of nodules in the image of the inset of Figure 2a is shown in Figure 3a. The mean diameter of individual nodules was about 250 nm and showed a reasonably narrow distribution (the standard deviation was 35 nm), suggesting a rela-

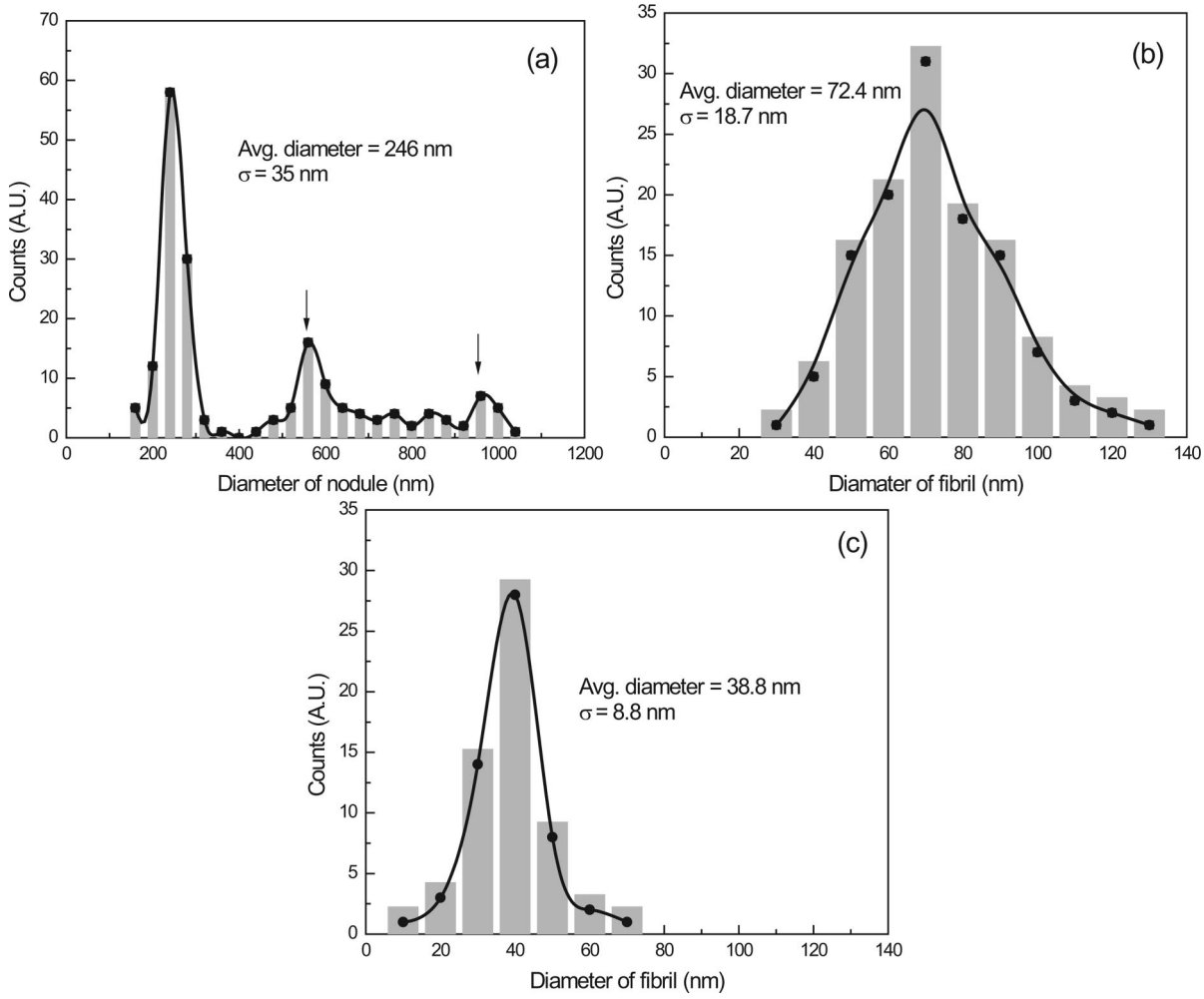

Figure 3. Size distribution of the diameter of (a) nodules of C-PEDOT at T_{sub} = 20 °C and fibrils of C-PEDOT at (b) T_{sub} = 50 °C and (c) T_{sub} = 80 °C. Arrows denoted in (a) represent the peak position of merged nodules.

tively constant rate of gas evolution and effusion during the deposition. The distribution could not be fitted with one Gaussian curve, and the distribution had some separate, additional peaks with a size of greater than 500 nm, which clearly supports the hypothesis of formation of larger nodules by merging individual nodules of uniform size distribution.

At higher substrate temperatures, the rapidly growing film temporarily entrains the gaseous byproduct, which is finally released through the burst of vapor bubbles over the entire surface of the film (Figure 2b,c). This vigorous effusion not only enlarged the pore size in the film but also added mechanical stress to the fibril. Consequently, the fibril diameter decreased significantly (20−60 nm), and the length of the fibril increased. Some of the fibril texture was disconnected by the mechanical stress of the gaseous byproduct effusion, causing pores to merge and increasing the overall porosity of the film. The size distributions of fibrils in Figure 2b,c demonstrate narrow Gaussian curves (Figure 3b,c). At T_{sub} = 50 °C, the mean diameter of fibrils was about 72 nm, which became thinner (mean diameter = 39 nm) with narrower distribution at T_{sub} = 80 °C. The estimated rms roughness of C-PEDOT at T_{sub} = 50 °C was more than 20 nm, and the depth of the pore was generally larger than 50 nm. Considering the total film thickness measured by profilometry was 75 nm, it follows that the interconnected texture structure was maintained throughout the thickness of C-PEDOT film. The SEM images (Figure 2b,c) of the nanoporous structure in C-PEDOT deposited at higher substrate temperatures also strongly support the hypothesis that a gaseous vapor evolved out from the solid PEDOT surface as bubbles during the oCVD process. Moreover, the observed size distribution infers that the rate of vapor effusion was relatively constant with respect to T_{sub}, which strongly suggests that the nanoporous structure can be tuned systematically by controlling T_{sub} during the oCVD process. Analogous porous structures in other materials are formed by the mechanism of gas evolution. For example, Styrofoam, a well-known packaging material, is produced by the thermal expansion of a gaseous blowing agent such as pentane or CO_2 in solid polystyrene. Another well-known example is basalt, which is formed by the rapid cooling of lava at the surface of earth (Figure 2b, inset). The en-

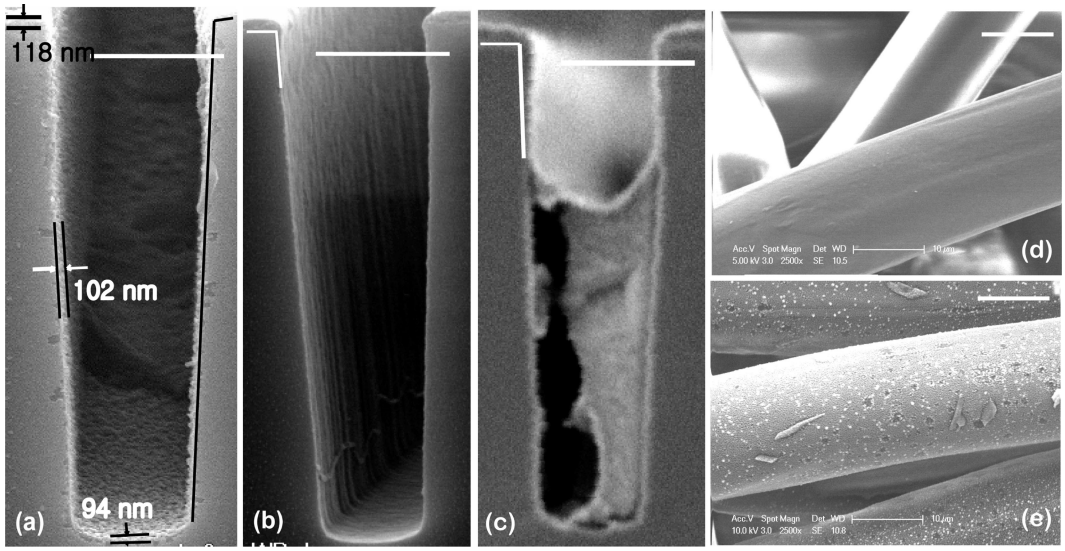

Figure 4. Cross-sectional SEM images of (a) C-PEDOT and (b) F-PEDOT deposited on the trenches, and (c) EDOT and $FeCl_3$ mixture solution was spin-cast to form highly anisotropic PEDOT on the trench. Each scale bars represents 2 μm. Black line in the right side of (a) and white line in the left side of (b) and (c) show the borders between the Si trench and C-PEDOT film. SEM images of conformally coated C-PEDOT film on a paper mat (d) before and (e) after the deposition of C-PEDOT film. Each scale bars represents 10 μm.

trapped water or air vapor in solidified lava results in the characteristic porous structure of basalt, which has morphological similarity to the surface structure of C-PEDOT.

In the case of F-PEDOT, the strong oxidant $FeCl_3$ can oxidize EDOT so quickly that the rate of gaseous byproduct release is much faster than that of condensation of PEDOT film. Therefore, gaseous HCl can easily escape at the surface of formed PEDOT, and smooth F-PEDOT is formed by the oCVD process (Figure 2d). In other words, the nanoporous structure can be formed in the course of competing process of oxidation reaction and condensation, and it follows that the slow oxidation reaction with $CuCl_2$ plays a critical role in forming this basalt-like structure.

Conformal Coverage on Complex Geometries. In addition to resulting in different surface morphologies on flat substrates, the change in oxidants impacts the degree of conformality over nonplanar microstructured substrates. Trenches (8 μm deep × 2 μm wide) in silicon were used to examine the conformal coverage of oCVD PEDOT grown with different oxidants at substrate temperatures less than 100 °C. Figure 4a,b demonstrates the cross-sectional SEM images of C-PEDOT (a) and F-PEDOT (b) on these standard trenches deposited at T_{sub} = 50 °C. For F-PEDOT, the vaporized $FeCl_3$ has very high sticking probability, nearing unity, because it is almost nonvolatile at T_{sub} less than 100 °C.[17] Since the evaporated $FeCl_3$ from the heating crucible is directional, most of $FeCl_3$ is condensed near the entrance region of the trench. The resultant cross-sectional image clearly shows that F-PEDOT was deposited mostly on the entrance of the trench and no film was observed at the bottom and the side wall of the trench. On the other hand, the oCVD of C-PEDOT involves highly volatile Cl_2 vapor in the deposition process. Cl_2 has much lower sticking probability compared with $FeCl_3$ vapor due to extremely high volatility. The lower sticking probability allows nondirectional flux of oxidant in the trench, which can be materialized as a conformal coverage of the trench.[17] Figure 4a demonstrates the conformal growth of about 120 nm thick C-PEDOT in the trench. The nanoporous, basalt-like structure could be observed in both side walls and the bottom of the nanometer scale conformally covered trench. Although the oCVD procedure is almost the same between C-PEDOT and F-PEDOT, the dramatic difference in conformality supports the hypothesis of the involvement of volatile Cl_2 in C-PEDOT deposition, which is one of the unique advantages that the $CuCl_2$ oxidant can offer. This conformal coverage is a unique property of the CVD process, which is very difficult to achieve in other liquid phase based methods.[17] For comparison, Figure 4c shows the result of spin-casting and polymerizing a liquid phase mixture of EDOT and $FeCl_3$ solution in methanol is an extremely nonconformal coverage. The solution was trapped at the bottom of the trench but depleted at the side wall and upper mouth area. The resultant feature was highly irregular compared to the original shape of trench.

The conformal coverage can also be achieved on various convex and concave surfaces. Since oCVD is a vapor phase based process, oCVD PEDOT can be conformally deposited on various soft, vulnerable substrates without damaging the substrate structure. Figure 4e demonstrates the C-PEDOT deposited at T_{sub} = 80 °C on a paper mat whose fiber diameter was 15−25 μm long. The SEM images showed that C-PEDOT was conformally deposited around the fibers of the paper mat while maintaining the initial features of the mat. The nanostructure of C-PEDOT was also observed at the surface of the microstructured paper mat. Combined

with the microstructure offered from the paper mat, the nanostructure from C-PEDOT on the paper mat has a hierarchical, huge surface area, advantageous for various applications such as flexible electrodes with high surface areas and supercapacitors.

Superhydrophobicity and Oil Repellency. One of the properties that the nanoporous structure can affect is wettability.[6,25−28] On a smooth, flat, and chemically homogeneous surface, the contact angle, θ, is defined by Young's equation

$$\cos\theta = \frac{\gamma_{SV} - \gamma_{SL}}{\gamma_{LV}} \quad (1)$$

where γ_{SV}, γ_{SL}, γ_{LV} is solid−vapor, solid−liquid, and liquid−vapor interfacial tension, respectively. In Young's equation, θ is solely determined by the chemical composition of solid, liquid, and vapor involved. When the surface is roughened, the apparent contact angle (θ^{app}) can be altered by a geometric factor, given by Wenzel's equation

$$\cos\theta^{app} = r\cos\theta \quad (2)$$

where *r* is a ratio of true surface area to the horizontal projection of surface area.[25,27] Assuming the chemical composition of the surface is identical, the θ^{app} can be modulated solely by altering the surface morphology. If θ is less than 90°, θ^{app} is always less than θ because *r* in eq 2 is always larger than 1. Therefore, if the flat surface is hydrophilic, the roughened surface becomes more hydrophilic and the surface is more wettable.

The effect of high surface roughness on C-PEDOT on wettability was evaluated by measuring θ for water (Figure 5a−c) on the surface. Compared to the contact angle of F-PEDOT whose surface roughness is relatively low (Figure 5a), the contact angle of C-PEDOT displays a large decrease of contact angle (Figure 5b,c). As the rms roughness increases, the contact angle decreases significantly. Considering that the chemical compositions of F-PEDOT and C-PEDOT are almost identical, the contact angle difference mainly derives from morphological effect. With a surface roughness of higher than 40 nm, the contact angle of C-PEDOT surface is 10°, which is very close to being superhydrophilic.

Analogously, if the γ_{SV} is smaller than γ_{SL} in eq 1, then contact angle (CA) is greater than 90° and the θ^{app} with the roughness of *r* is greater than θ of a flat surface, according to eq 2. As the morphology of the C-PEDOT surface is significantly rough, the surface can be rendered strongly hydrophobic by coating with a low surface energy material. For this purpose, a 25 nm thick fluorinated acrylate (poly(perfluorodecyl acrylate), PFA) polymer film with low surface energy (γ_{SV} = 9.3 mN/m) was deposited *via* initiative chemical vapor deposition (iCVD).[26,27] The CA of water on PFA-modified F-PEDOT was 120°, which was similar to the contact angle of water on a pure PFA film, 118° (Figure 5d).[26] On the other hand, a 120 nm thick nanoporous C-PEDOT film coated with 25 nm of PFA showed a large increase in contact angle, to 150 ± 3°, which is close

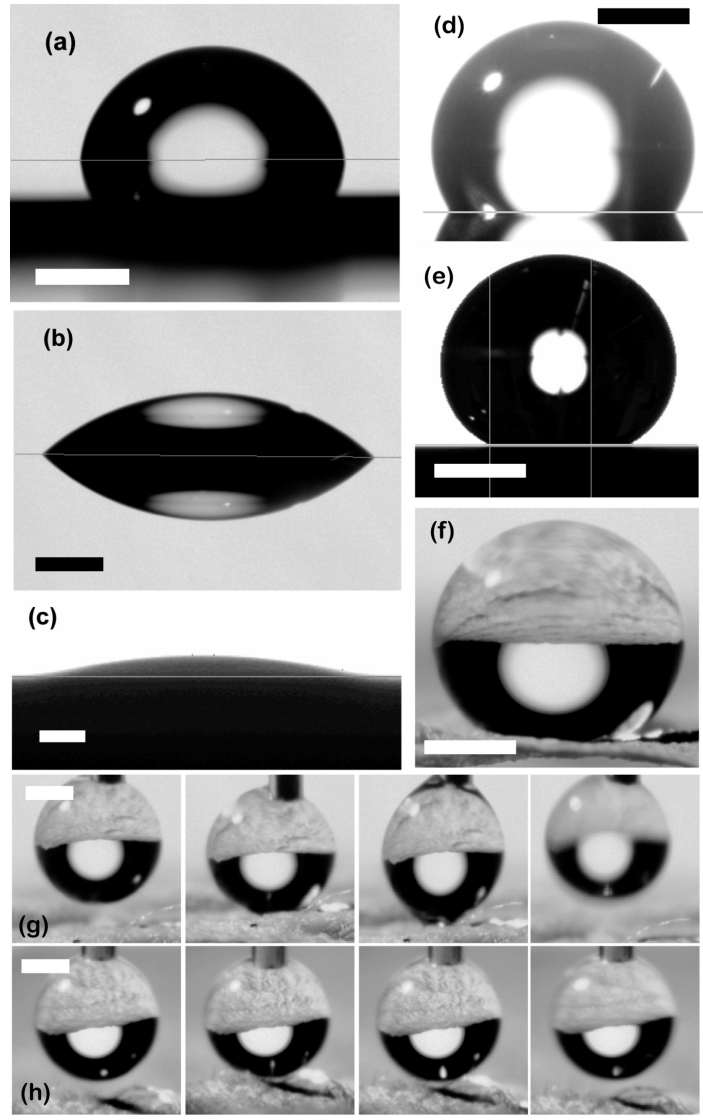

Figure 5. Water droplet contact angle variations of PEDOT film according to the surface roughness; (a) F-PEDOT, rms roughness = 3.7 nm, θ = 84°; (b) C-PEDOT, rms roughness = 22.7 nm, θ = 37°; (c) C-PEDOT, rms roughness = 43.0 nm, θ = 10°. Contact angle variations of PFA-modified PEDOT film; (d) F-PEDOT, θ = 120°; (b) C-PEDOT, θ = 150°. (f) Digital camera image of PFA-modified C-PEDOT coated paper mat. A series of pictures captured from a CCD camera for an advancing and receding water droplet on (g) a PFA-modified paper mat and (h) a PFA-modified C-PEDOT-coated paper mat, respectively. Each scale bar represents 1 mm.

to a superhydrophobic surface (Figure 5e).[27] Neither the surface morphology of the basalt-like structure nor the conductivity of the C-PEDOT film was significantly altered by subsequent iCVD deposition. Since the iCVD PFA film was conformally covered with both C-PEDOT and F-PEDOT films, the chemical composition of surface is practically identical,[26] and the increase of contact angle in C-PEDOT is solely due to the nanoporous, textured morphology.

If a surface shows superhydrophobicity ($\theta > 150°$), the water is believed to form a composite interface with the surface texture, termed the Cassie regime.[25,27] In the Cassie regime, θ^{app} is calculated as the average of θ of the solid and the air, given by

$$\cos \theta^{app} = -1 + \varphi_s(1 + \cos \theta) \quad (3)$$

where ϕ_s is the fraction of solid−liquid contact area.[25] When the surface texture is so rough that the water cannot penetrate into the valleys of the structure, small pockets of air become entrapped and the water sits partially on air. If the area ratio of the air region over surface is close to 1, the composite interface between water/solid/air becomes practically air-like, which is extremely hydrophobic and exhibits very low hysteresis. By combining our nanoscale roughness with the microscale textures of the paper mat, the C-PEDOT surface could be made even more hydrophobic. This is actually the technique used by the famous lotus leaf.[28] As shown in Figure 4d, the one-step oCVD process can easily form a hierarchical structure of nanometer scale roughness of C-PEDOT on the micrometer scale roughness of the paper mat.

Although the exact value of θ^{app} was difficult to determine because the extremely rough surface of the paper mat made it difficult to obtain a flat baseline for the contact angle measurement (Figure 5f), the measured contact angle was higher than 163°. Moreover, the water droplet was not pinned on the C-PEDOT coated paper mat and showed negligible hysteresis. A series of pictures were captured to elucidate the hysteresis of advancing and receding water droplet on PFA-modified paper mat as a control (termed as control mat afterward, Figure 5g) and C-PEDOT-paper mat (termed as sample mat afterward, Figure 5h). The highly microporous control mat resulted in the Cassie state when a water droplet was applied. No increase in the advancing contact angle was observed when the water droplet was pressed on the mat. However, a decrease in the receding contact angle was clearly observed when the water droplet was siphoned from the control mat. Although the water sits on the air in the microscale pores between fibers, a considerable amount of control mat area was in contact with the water droplet. Hence, in spite of the low surface energy of PFA film, the wet area can be pinned adhesively with a water droplet, which possibly caused the receding angle hysteresis in the control mat.[25] On the other hand, the sample mat has an enormously tortured surface area in nanometer scale, compared with the control mat. With this nanoscale surface curvature, penetration of water into the microscale is even further reduced, which greatly decreases the contact surface area, ϕ_s in eq 3. Consequently, adhesive pinning[25] is greatly depressed, and the sequential CCD camera images clearly show no hysteresis between advancing and receding angles.

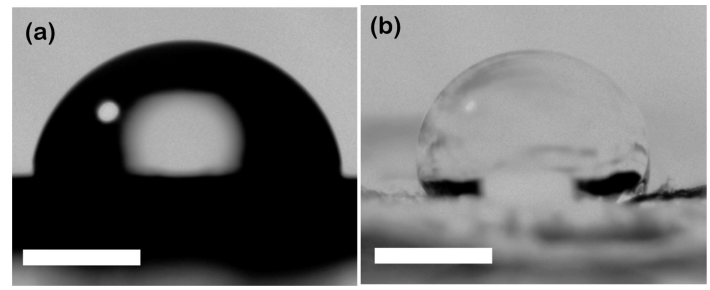

Figure 6. Ethanol droplet contact angles on (a) PFA-modified C-PEDOT film on a Si wafer (θ = 88°) and (b) PFA-modified C-PEDOT coated paper mat (θ = 113°). Each scale bar represents 1 mm.

Furthermore, the oil repellency—termed as oleophobicity—could also be observed from PFA-modified C-PEDOT film on a Si wafer (Figure 6a) and a sample mat (Figure 6b). Since the surface tension of most oil is generally much lower than that of water (γ_{LV} = 71.99 mN/m at 25 °C),[22] it is extremely difficult to achieve oleophobicity.[27,28] The contact angle of ethanol droplet (γ_{LV} = 21.97 mN/m at 25 °C)[22] on PFA-modified C-PEDOT film on a Si wafer was 88° (Figure 6a), which is almost 2-fold greater than the CA of flat PFA-coated Si wafer (43°), which shows that the surface roughness of C-PEDOT plays a critical role in the oil repellency. According to eq 2, θ^{app} of an ethanol droplet in Figure 6a should decrease since θ of the ethanol droplet is less than 90°. However, the observed result is reversed, which might be from the metastable Cassie state or local pinning effect in the Wenzel state.[28] The receding angle from this droplet was practically 0°, which can occur also from both the highly hysteric Cassie state or the strongly textured Wenzel state. To investigate this aspect further, we have deposited ethanol on the sample mat. Ethanol did not penetrate into the fabrics, which conclusively supports the formation of the Cassie state on the sample mat, and θ^{app} was 113°. The observed water and oil repellency of the highly conductive PEDOT film can greatly enhance the self-cleaning ability, which potentially has a wide impact on anticorrosion and antifouling from polluted water and fatty liquid.[28]

CONCLUSION

In conclusion, a new nanostructured PEDOT film was obtained *via* an oCVD process by introducing the new oxidant of $CuCl_2$. The obtained C-PEDOT film showed high electrical conductivity up to 32 S/cm. Substrate tem-

perature was a critical process parameter in oCVD that controls the conductivity of the C-PEDOT film, as was the same in F-PEDOT. A basalt-like nanoporous structure was uniformly obtained from C-PEDOT deposited at T_{sub} higher than 50 °C. The pore size and porosity could be systematically tuned by modulating substrate temperature. The C-PEDOT film showed ultimately improved conformality on the substrate. Conformal coverage on the standard trench in Si and on the paper fiber mats was clearly visible in the SEM images with retention of the complex surface structure. As an example of the effect of morphology, the contact angle decreases according to increase of the surface roughness, and an extremely hydrophilic surface was successfully obtained. Moreover, on microstructured substrates, highly conductive and superhydro/oleophobic surfaces, such as nonwettable conducting paper, could also be obtained easily by subsequent oCVD and iCVD processes. The regularly nanostructured, hierarchical nanostructure has great potential for a variety of applications. For instance, highly hydrophilic conductive PEDOT film can be used for advanced electrochemical applications, such as biosensors. Achieving a high surface area layer on planar substrates and conformal coating of high surface area substrates enable features for devices such as supercapacitor and batteries, where high interfacial area is desired.

METHODS

The detailed procedure of the oCVD process and the reactor configuration are described in detail elsewhere.[13−16] Si wafers, quartz plates, and paper were used as substrates for the oCVD of PEDOT. To monitor conformality, PEDOT was deposited on trenches with various aspect ratios patterned on a Si wafer, which were supplied from Analog Devices. Process pressure was maintained between 50 and 100 mTorr, and the flow rate of evaporated EDOT monomer was metered through a mass flow controller at 5 sccm. The substrate temperature was varied between 20 and 100 °C by a PID controller. The oxidizing agent was evaporated from a resistively heated crucible. For C-PEDOT films, the oxidizing agent was $CuCl_2$ and was evaporated at a temperature greater than 380 °C. For F-PEDOT films, the oxidizing agent was $FeCl_3$ and was evaporated at 300 °C.

The total deposition time was 60 min. The thickness of PEDOT was controlled by the loading amount of $CuCl_2$ and the deposition time. After deposition, the film was rinsed with methanol for about 30 min to remove any residual oxidizing agent and EDOT monomer.

The iCVD process was also described in detail elsewhere.[27] Perfluorodecyl acrylate monomer and *tert*-butyl peroxide initiator were vaporized at room temperature and introduced into the iCVD chamber at flow rates of approximately 0.3 and 1.3 sccm, respectively. The polymerization reaction was initiated by heating a filament array to 280 °C. The process pressure was controlled at 100 mTorr by a throttling butterfly valve. Film thicknesses were monitored *in situ* by interferometry; approximately 25 nm of the PFA film was deposited in 10 min.

PEDOT film thickness was measured with a profilometer (Tencor, P-10), and the sheet resistance was measured with a four-point probe (MWP-6, Jandel Engineering Ltd.). The conductivity was calculated from the sheet resistance and measured thickness. FTIR spectra were collected on a Nexus 870, Thermo Electron Corporation. The surface morphology of PEDOT film was imaged by both SEM (FEI/Philips XL30 FEG ESEM) and AFM (Dimension 3100, Digital Instruments, Ltd.). The sampling size of roughness of PEDOT film was fixed at $2 \times 2\ \mu m^2$. The static contact angle was measured within 30 s after placing 2−4 μL of deionized water and ethanol droplets on the substrates (VCA2000, AST Inc.).

All chemicals were purchased from Aldrich and used without any further purification.

Acknowledgment. This research was supported by the U.S. Army through the Institute for Soldier Nanotechnologies, under Contract DAAD-19-02-D-0002 with the U.S. Army Research Office. The authors thank Edward F. Gleason in Analog Devices for the supply of trench wafers.

REFERENCES AND NOTES

1. Murray, C. B.; Kagan, C. R.; Bawendi, M. G. Synthesis and Characterization of Monodisperse Nanocrystals and Close-Packed Nanocrystal Assemblies. *Annu. Rev. Mater. Sci.* **2000**, *30*, 545–610.
2. Park, J.; An, K. J.; Hwang, Y. S.; Park, J. G.; Noh, H. J.; Kim, J. Y.; Park, J. H.; Hwang, N. M.; Hyeon, T. Ultra-Large-Scale Syntheses of Monodisperse Nanocrystals. *Nat. Mater.* **2004**, *3*, 891–895.
3. Langer, R.; Peppas, N. A. Advances in Biomaterials, Drug Delivery, and Bionanotechnology. *AIChE J.* **2003**, *49*, 2990–3006.
4. Sarikaya, M.; Tamerler, C.; Jen, A. K. Y.; Schulten, K.; Baneyx, F. Molecular Biomimetics: Nanotechnology through Biology. *Nat. Mater.* **2003**, *2*, 577–585.
5. Jang, J. Conducting Polymer Nanomaterials and Their Applications. *Emissive Materials: Nanomaterials* **2006**, 189–259.
6. Chiou, N. R.; Lui, C. M.; Guan, J. J.; Lee, L. J.; Epstein, A. J. Growth and Alignment of Polyaniline Nanofibres with Superhydrophobic, Superhydrophilic and Other Properties. *Nat. Nanotechnol.* **2007**, *2*, 354–357.
7. Groenendaal, L.; Zotti, G.; Aubert, P. H.; Waybright, S. M.; Reynolds, J. R. Electrochemistry of Poly(3,4-Alkylenedioxythiophene) Derivatives. *Adv. Mater.* **2003**, *15*, 855–879.
8. Groenendaal, B. L.; Jonas, F.; Freitag, D.; Pielartzik, H.; Reynolds, J. R. Poly(3,4-Ethylenedioxythiophene) and Its Derivatives: Past, Present, and Future. *Adv. Mater.* **2000**, *12*, 481–494.
9. Jang, J.; Chang, M.; Yoon, H. Chemical Sensors Based on Highly Conductive Poly(3,4-Ethylenedioxythiophene) Nanorods. *Adv. Mater.* **2005**, *17*, 1616–1620.
10. Sotzing, G. A.; Briglin, S. M.; Grubbs, R. H.; Lewis, N. S. Preparation and Properties of Vapor Detector Arrays Formed from Poly(3,4 Ethylenedioxy)thiophene-poly(styrene sulfonate) Insulating Polymer Composites. *Anal. Chem.* **2000**, *72*, 3181–3190.
11. Sirringhaus, H.; Kawase, T.; Friend, R. H.; Shimoda, T.; Inbasekaran, M.; Wu, W.; Woo, E. P. High-Resolution Inkjet Printing of All-Polymer Transistor Circuits. *Science* **2000**, *290*, 2123–2126.
12. Abidian, M. R.; Kim, D. H.; Martin, D. C. Conducting-Polymer Nanotubes for Controlled Drug Release. *Adv. Mater.* **2006**, *18*, 405–409.
13. Im, S. G.; Gleason, K. K. Systematic Control of the Electrical Conductivity of Poly(3,4-Ethylenedioxythiophene) *via* Oxidative Chemical Vapor Deposition (oCVD). *Macromolecules* **2007**, *40*, 6552–6556.
14. Im, S. G.; Olivetti, E. A.; Gleason, K. K. Doping Level and Work Function Control in Oxidative Chemical Vapor Deposited Poly(3,4-Ethylenedioxythiophene). *Appl. Phys. Lett.* **2007**, *90*, 152112.
15. Im, S. G.; Yoo, P. J.; Hammond, P. T.; Gleason, K. K. Grafted Conducting Polymer Films for Nano-Patterning onto Various Organic and Inorganic Substrates by Oxidative

Chemical Vapor Deposition. *Adv. Mater.* **2007**, *19*, 2863–2867.
16. Lock, J. P.; Im, S. G.; Gleason, K. K. Oxidative Chemical Vapor Deposition of Electrically Conducting Poly(3,4-Ethylenedioxythiophene) Films. *Macromolecules* **2006**, *39*, 5326–5329.
17. Gates, S. M. Surface Chemistry in the Chemical Vapor Deposition of Electronic Materials. *Chem. Rev.* **1996**, *96*, 1519–1532.
18. Tran-Van, F.; Garreau, S.; Louarn, G.; Froyer, G.; Chevrot, C. Fully Undoped and Soluble Oligo(3,4-Ethylenedioxythiophene)s: Spectroscopic Study and Electrochemical Characterization. *J. Mater. Chem.* **2001**, *11*, 1378–1382.
19. Skotheim, T. A.; Elsenbaumer, R. L.; Reynolds, J. R. *Handbook of Conducting Polymers*; M. Dekker: New York, 1998; pp1097−1225.
20. Im, S. G.; Olivetti, E. A.; Gleason, K. K. Systematic Control of the Electrical Conductivity of Poly(3,4-Ethylenedioxythiophene) *via* Oxidative Chemical Vapor Deposition (oCVD). *Surf. Coat. Technol.* **2007**, *201*, 9406–9412.
21. Baughman, R. H.; Shacklette, L. W. Conjugation Length Dependent Transport in Conducting Polymers from a Resistor Network Model. *J. Chem. Phys.* **1989**, *90*, 7492–7504.
22. Lide, D. R. *CRC Handbook of Chemistry and Physics*; Taylor and Francis Group, LLC: Boca Raton, FL, 2008.
23. Cotton, F. A.; Wilkinson, G. *Advanced Inorganic Chemistry: A Comprehensive Text*; John Wiley and Sons: New York, 1998.
24. Sadki, S.; Schottland, P.; Brodie, N.; Sabouraud, G. The Mechanisms of Pyrrole Electropolymerization. *Chem. Soc. Rev.* **2000**, *29*, 283–293.
25. Lafuma, A.; Quere, D. Superhydrophobic States. *Nat. Mater.* **2003**, *2*, 457–460.
26. Ma, M. L.; Gupta, M.; Li, Z.; Zhai, L.; Gleason, K. K.; Cohen, R. E.; Rubner, M. F.; Rutledge, G. C. Decorated Electrospun Fibers Exhibiting Superhydrophobicity. *Adv. Mater.* **2007**, *19*, 255–259.
27. Ma, M. L.; Mao, Y.; Gupta, M.; Gleason, K. K.; Rutledge, G. C. Superhydrophobic Fabrics Produced by Electrospinning and Chemical Vapor Deposition. *Macromolecules* **2005**, *38*, 9742–9748.
28. Tuteja, A.; Choi, W.; Ma, M. L.; Mabry, J. M.; Mazzella, S. A.; Rutledge, G. C.; McKinley, G. H.; Cohen, R. E. Designing Superoleophobic Surfaces. *Science* **2007**, *318*, 1618–1622.